Magnetic nanoribbons with embedded cobalt grown inside single-walled carbon nanotubes

*Denis M. Krichevsky[1,2], Lei Shi[3], Vladimir S. Baturin[4,5], Dmitry V. Rybkovsky[5], Yangliu Wu[3], Pavel V. Fedotov[1,6], Elena D. Obraztsova[1,6], Pavel O. Kapralov[2], Polina V. Shilina[2], Kayleigh Fung[7], Craig T. Stoppiello[7,8], Vladimir I. Belotelov[2,9], Andrei Khlobystov[7], Alexander I. Chernov[1,2,10]**

[1]Center for Photonics and 2D Materials, Moscow Institute of Physics and Technology (MIPT), Dolgoprudny, 141701, Russia

[2]Russian Quantum Center, 30, Bolshoy Bulvar, building 1, Skolkovo Innovative Center, Moscow region, 143026, Russian Federation

[3]State Key Laboratory of Optoelectronic Materials and Technologies, Nanotechnology Research Center, Guangzhou Key Laboratory of Flexible Electronic Materials and Wearable Devices, School of Materials Science and Engineering, Sun Yat-sen University, Guangzhou 510275, P. R. China

[4]Vernadsky Institute of Geochemistry and Analytical Chemistry of Russian Academy of Sciences, 19, Kosygina street, Moscow, 119991, Russia

[5]Skolkovo Institute of Science and Technology, 3, Nobel street, Moscow, 143026, Russian Federation

[6]A. M. Prokhorov General Physics Institute, Russian Academy of Sciences, 38, Vavilov street, Moscow, 119991, Russian Federation

[7]School of Chemistry, University of Nottingham, University Park, Nottingham, NG7 2RD, UK

[8]Nanoscale and Microscale Research Centre, University of Nottingham, University Park, Nottingham, NG7 2RD, UK

[9]Photonic and Quantum technologies school, Lomonosov Moscow State University, Leninskie gori, 119991 Moscow, Russia

[10]NTI Center for Quantum Communications, National University of Science and Technology MISiS, 4, Leninskiy pr., Moscow, 119049, Russia

KEYWORDS nanoribbon, phthalocyanine, Raman spectroscopy, carbon nanotube, carbon nanomaterials

ABSTRACT Molecular magnetism and specifically magnetic molecules are recently gaining plenty of attention as key elements for quantum technologies, information processing, and spintronics. Transition to the nanoscale and implementation of ordered structures with defined parameters is crucial for advanced applications. Single-walled carbon nanotubes (SWCNTs) provide a natural one-dimensional confinement that can be implemented for encapsulation, nano synthesis, and polymerization of molecules into nanoribbons. Recently, the formation of atomically precise graphene nanoribbons inside the SWCNTs has been reported. However, there have been only a limited amount of approaches to form ordered magnetic structures inside the nanotube channels and the creation of magnetic nanoribbons is still lacking. In this work we synthesize and reveal the properties of cobalt-phthalocyanine based nanoribbons (CoPcNRs)

encapsulated in SWCNTs. Raman spectroscopy, transmission electron microscopy, absorption spectroscopy, and density functional theory calculations allowed us to confirm the encapsulation and to reveal the specific fingerprints of CoPcNRs. Magnetic properties were studied by transverse magnetooptical Kerr effect measurements and indicated the strong difference in comparison with the pristine unfilled SWCNTs due to the impact of Co incorporated atoms. We anticipate that this approach of polymerization of encapsulated magnetic molecules inside the SWCNTs will result in a diverse class of protected low-dimensional ordered magnetic materials for applications.

Introduction

Recent advances in the design, synthesis and characterization of molecular materials provide new perspectives in the fields of quantum technologies, information processing[1], sustainable energy[2], electronics[3], and spintronics[4]. Phthalocyanine molecules have already been widely used in the field of molecular magnetism due to several aspects, including: tunable properties, high temperature and chemical stability, planar configuration, and self-assembly, all leading to convenient device integration. Metal phthalocyanine complexes are composed of a phthalocyanine molecule and a metal ion that is located at its core. Variations of the central metal atoms provide variable electronic properties of the metallorganic complex. Magnetic properties depend on the metal ion electronic ground state[5] that is related to the interaction with the organic ligand. Overall, the properties are affected by the polymorphism resulting in diversity for single molecules, thin films, and bulk crystals for the compounds with identical metal ions. Electron spins of phthalocyanine molecules have found applications in the field of spintronics, to provide the tunnelling magnetoresistance effect[6] or spinterface effects[7]. In the latter effect, the spin polarization of the current from the ferromagnetic electrode is influenced by the molecular layer at the interface. Moreover, the single-molecule level devices become feasible, and the spin

manipulation is performed within the nanotransistor electrically[8] or via scanning tunnelling microscopy[1].

Phthalocyanine based structures hold a strong promise for quantum information processing as molecular spin qubits[9] bolstered by the long coherence times[10] at liquid nitrogen temperatures superior to many molecular systems. The experimental realization of logical operations with molecules has been demonstrated[1,11]. However, the real implementation of quantum computing on those systems indeed is facing limitations, including the challenges for simultaneous wiring of several qubits together with sustenance of long coherence times. The relaxation processes, such as Orbach spin-phonon interaction process, come to the focus of attention[12]. Simultaneously placing the molecules with nanometer accuracy together with the control over the electronic structure of the molecular nanomagnets is vital and has hardly been accessed yet. Encapsulation inside carbon nanostructures can be a successful route not only for constructing the functional quantum materials[13], but also for improving the properties of magnetic species due to alignment inside the 1D channels[14–16].

Single-walled carbon nanotubes (SWCNTs) are well-known for their ability to encapsulate guest structures and to be used as a template for synthesis at the nanoscale[17]. Various types of compounds have been successfully encapsulated and formed inside the nanotube channels, including magnetic nanostructures[18–20]. The diameter of the nanotube is the foremost parameter that specifies the filling process[21] in terms of encapsulation ability and type of the resulting nanostructure that can be formed inside. In example, for the case of coronene ($C_{24}H_{12}$), a polycyclic aromatic hydrocarbon (PAH) molecule, encapsulation can result in the formation of the molecules stacks oriented at different angles with respect to the nanotube axis[22,23] or in polymerization into nanoribbons (NR) that are in general formed in larger diameter tubes[24,25]. Graphene nanoribbons (GNRs) with sub-

nanometer widths are attracting much attention since they are able to provide a substantially large band gap opening in the electronic structure, which is advantageous for nanoscale applications. In addition to the bottom-up approach[26,27] that is limited to the on-surface synthesis and to only specific precursors that can be used, GNRs can be specifically formed inside the nanotubes. Growth inside the nanotube channels is advantageous since various molecules can be used including fullerenes[28], PAH[17], ferrocenes[29] resulting in formation of long and narrow GNRs with various geometries. Recent experiments combining transmission electron microscopy and multi wavelength Raman spectroscopy unambiguously prove the formation of highly uniform GNRs with identical properties inside the nanotubes[29]. However, magnetic NR formed inside the nanotubes, a material that can be perspective for quantum technologies, were not demonstrated by far. While the bottom-up approach can result in the formation of GNRs with the nontrivial magnetic ground states[30], a complicated precursor synthesis routes provide limited amounts of the samples and hamper the near-term implementation of the material.

In this work we study the magnetic nanoribbons formed from cobalt phthalocyanine (CoPc) molecules inside the SWCNTs. High resolution transmission electron microscopy reveals the successful filling of the nanotubes and formation of long 1D structures inside. We synthesize the material at various temperature conditions and utilize Raman spectroscopy to reveal the unique phonon vibrations that correspond to CoPcNR. As a result, we validate the specific growth parameters for CoPcNR formation. Density functional theory (DFT) calculations provide the assumptions for the type of the characteristic modes in the CoPcNRs. We follow the optical response modification of the phthalocyanine molecules upon the nanotube incorporation and further polymerization into CoPcNRs and detect the peculiar features in the absorption and Raman spectra related to the NRs. Finally, we implement magneto optical Kerr effect measurements to

study the magnetic properties at room temperature. CoPcNRs formed from polymerized CoPc molecules demonstrate magnetic response which significantly differs from the pristine host SWCNTs. The 1D material can be treated with the known approaches that are well approved for carbon nanotubes. We believe, that synthesis of magnetic CoPcNRs inside the protected channels of nanotubes can provide a new platform for the applications.

Results and discussion

CoPcNR structure

We use the two-step approach for synthesis of nanoribbons. First, the filling of SWCNTs with CoPc molecules was performed at 375 °C within the sealed glass ampules. Inside narrower nanotubes, CoPc molecules were observed to form stacks as shown by high resolution transmission electron microscopy (HR-TEM) imaging (Fig. S5). At the second step, the polymerization of the molecules encapsulated in SWCNT was performed at higher temperatures (400 - 700 °C) which resulted in the formation of twisted ribbons (Fig.1a and Fig. S4). Metal phthalocyanines have previously been reported to form nanowires with widths of hundreds of nanometers upon evaporation on various surfaces[31]. In our experiments, the formation of nanowires or other structures derived from CoPc outside of SWCNTs were not observed in the microscopy data.

In previous works, hydrogen-terminated GNRs formed inside of the SWCNTs were successfully imaged by HR-TEM, despite the electron beam damage[29]. In the case of sulfur terminated or chlorine terminated NRs, the edges of the encapsulated structures are more stable and can be resolved clearly in a zigzag configuration[32,33]. However, even when the exact atomic structure of the nanoribbon edge is not possible to be resolved by HR-TEM, the key structural characteristic is the helical twist, a result of nanoribbon confinement inside the nanotube, that allows distinguishing NR from encapsulated molecules or internal nanotube[32,34]. The nanoribbons derived from CoPc

in our experiments appear to possess the characteristic helical twists (Fig. 1a) originating due to the nanotube confinement[35]. The average width of the nanoribbons estimated from the TEM is 0.7 nm. Notably, the temperatures used for the filling protocols and further polymerization exclude the possibilities for the formation of double-walled carbon nanotubes, that generally require temperatures around 1000 °C. Complementary to the HR-TEM imaging, the local energy-dispersive X-ray (EDX) spectroscopy (Fig. S3) detects a signal of cobalt in the CoPcNR@SWCNT despite a very low atomic percent of this metal in the sample.

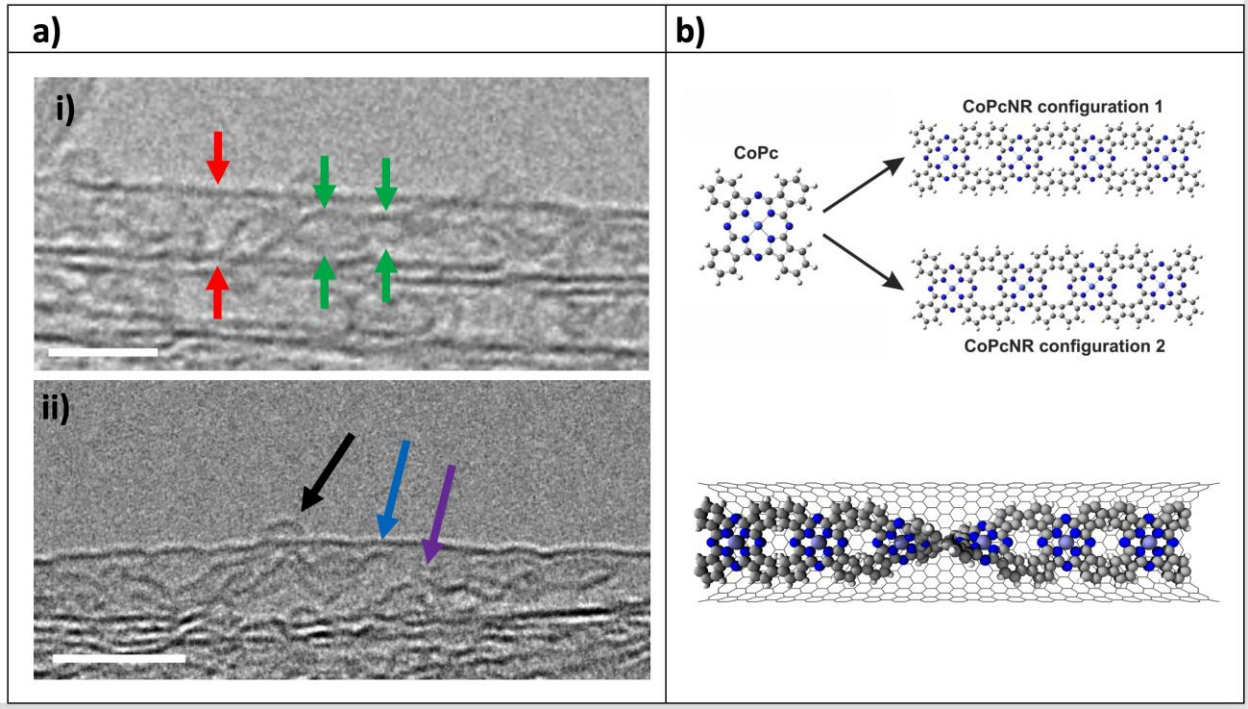

Figure 1. TEM images of the CoPcNR inside SWCNT and models of the structures that are considered in the experiment. a)_HR-TEM images of CoPcNR@SWCNT. i) The ribbon appears as a low contrast moiety with a width ranging between 0.6 and 0.8 nm (denoted by the green arrows) inside a 1.54 nm wide SWCNT (the walls are indicated by the red arrows); ii) In a separate SWCNT, both a face-on projection of the nanoribbon (blue arrow) and a twist (purple arrow) are visible. The black arrow denotes a small defect on the surface of the SWCNT. The polymerization

was performed at 450 °C. The scale bars are 2 nm. b) Possible pathways of polymerization of CoPc in nanotubes leading to two different structures of CoPcNR. Light blue central atom is Co, dark blue – nitrogen, grey – carbon, and white – hydrogen.

Based on the values of synthesis temperature, features observed in TEM images and possible ways of reacting of phthalocyanine rings which are constrained by the host-nanotube, we propose two types of NR structures that can be formed from CoPc molecules in nanotubes (Fig. 1b). The first one is obtained via the loss of two hydrogen atoms and cross-linking of the neighboring CoPc molecules through the C-C bonds. The second one is a more rigid structure where the additional two pairs of C-C bonds are formed. Both of the structures have specific areas where the twist is likely to occur. For instance, for the first structure the two clashing C-H bonds create tension. Molecular dynamics modelling showed that both of the proposed NR structures are possible in nanotubes of different diameters. However, as HR-TEM is not able to determine the structure of the nanoribbon precisely due to the structural complexity and lack of stability under the electron beam, we perform Raman spectroscopy and DFT modelling investigations to establish the nature of these materials.

Raman spectroscopy

Raman spectroscopy has recently been shown as a very effective tool for the investigation of atomically precise GNRs. In the case of surface bottom-up growth, laser excitation can be used for the direct driving of reactions and *in situ* analysis of the growth kinetics via the Raman intensities of the synthesized structures vibrations[27]. Encapsulated GNRs can also be successfully characterized with Raman spectroscopy. Despite the spectral range overlap between phonons of

NRs and SWCNTs it was possible to detect the difference in the spectra for the filled and empty nanotubes[24,25]. In the early works only a variation of the frequencies for the radial breathing modes of nanotubes were identified, caused by several factors including the stiffening of the nanotube vibration due to filling, and the appearance of a D prime band that can be attributed to the edge activation[36] of the nanoribbons. Recently, it was clearly demonstrated that the radial breathing like mode (RBLM), CH in-plane bending (CH-ipb) and D-like modes[37] can also be detected when the GNRs are inside the nanotubes[29]. Excitation wavelength resonant response enables the estimation of the electronic structure of the synthesized GNRs. Therefore, matching the resonant condition becomes crucial for the successful identification of formed NRs inside the SWCNT channels. In Fig. 2 we represent the Raman spectra of the pristine molecules, filled sample and heat-treated samples with grown NRs at different temperatures. It can be seen that starting from the temperatures around 400 °C and up to 600 °C new vibrations become active, in contrast to the filled sample, and vanish at higher temperatures which are closer to the regime when the double-walled carbon nanotubes can start to be formed[38]. The excitation wavelength of around 785 nm (1.58 eV) enables us to detect the response from the pristine CoPc molecules without a strong photoluminescence background and to compare this with the new Raman modes that appear during CoPcNRs formation. We note that higher frequency vibrations (1300-1550 cm^{-1}) get somewhat similar to the pristine CoPc case, although shifted in position. However, there are some clear differences namely the sharp narrow lines at around 458 cm^{-1}, CH-ipb mode at 1240 cm^{-1}, 1447 cm^{-1} and others in the D region, together with the well-pronounced 1542 cm^{-1} mode. The intensity of these peaks becomes maximal only in the specific synthesis thermal range (450-600 °C) and can be detected with resonant Raman conditions that are fulfilled at precise laser excitation wavelengths. Comparison with the similarly processed molecules on the quartz substrate, but

without SWCNTs didn't result in any similar Raman response. At low test temperatures (below 400 °C) only traces of molecules at the limit of detection can be found, but indeed, no phonon bands at 1542 or 457 cm^{-1}. We further focus our attention on the vibrations that appear after polymerization inside SWCNTs at 458 cm^{-1} that is close to the region of the RBLM in example for the 6 AGNR[29] and 7 AGNR[39], and 1542 cm^{-1} band. The narrow line width of the peak in RBLM region at 500 °C suggests that this temperature provides the synthesis conditions for CoPcNRs with a well-defined structure. In order to reveal the origin of the appearing phonon vibrations we performed the DFT modelling of the Raman spectra for polymerized CoPc molecules.

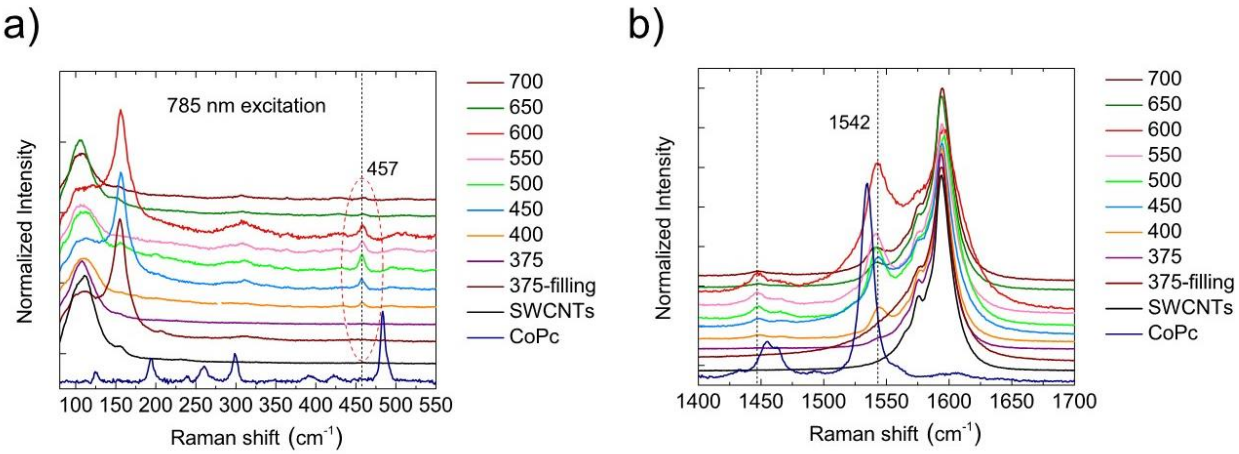

Figure 2. Raman spectroscopy and synthesis temperature ranges. The measurements were performed at 785 nm excitation wavelength. Blue color – CoPc molecules, black – pristine opened SWCNTs, color coded various temperatures of polymerizations. a) Low frequency range. Peaks positioned from 75 to 250 cm^{-1} are originating from the radial breathing modes of SWCNTs. Increase of intensities of several peaks at 155 cm^{-1} originate from resonantly excited specific geometries of nanotubes that are nonuniformly distributed on the samples. The characteristic band that is related to CoPcNRs is highlighted with the dashed circle (see main text). b) G-band region of SWCNTs. Main CoPcNR peaks are highlighted with the dashed vertical lines.

DFT simulation

To investigate the possible sources of the changes in the observed Raman spectra after sample heating, we performed computational modeling of different CoPc molecule configurations within the Gaussian package (the description of the computational methodology is given in the methods section). Prior to the estimation of the phonon bands, the stability of NR structures and behavior of the molecule relaxation inside SWCNT have been verified (Fig. S6). We first compare the computed Raman spectrum of an isolated molecule with the corresponding experimental spectrum. The B3LYP exchange-correlation functional overestimates the vibrational frequencies of CoPc. We found that the scaling factor of 0.98 results in better agreement of the peak positions with experimental data (outside of the most intense band at 1565 cm^{-1} which remains overestimated even after the scaling). Fig. 3 shows the comparison of the calculated and experimentally measured spectra for the isolated CoPc molecule.

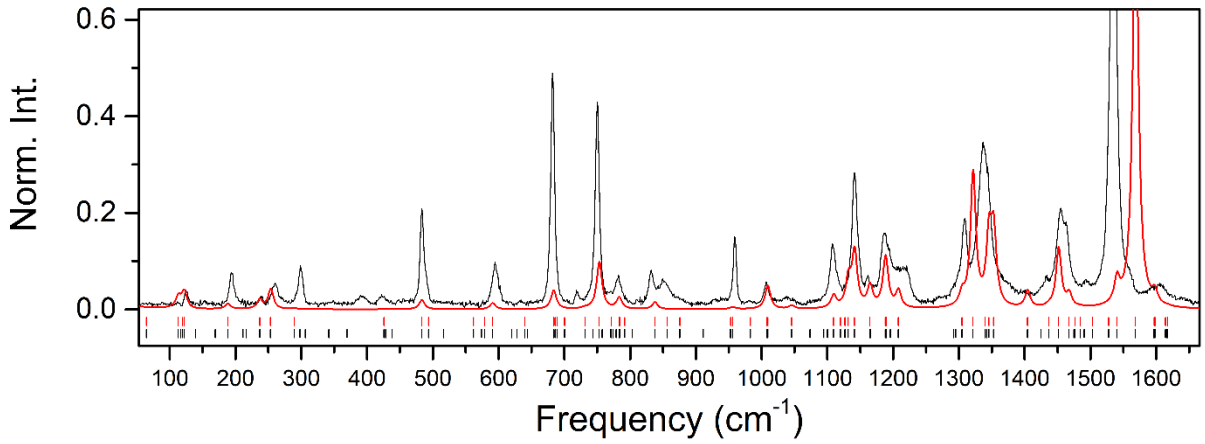

Figure 3. Calculated Raman spectrum of CoPc molecules. Comparison of the experimental (black line) and calculated (red line) Raman spectra of the CoPc molecules. The computed frequencies are scaled with a factor of 0.98. Red stripes below the spectra curves depict the calculated positions of vibrational modes with non-zero Raman intensities. Black stripes depict the positions of all calculated vibrational modes.

The red stripes below the plot illustrate the positions of the vibrational modes with non-zero Raman intensity, whereas black stripes depict the positions of all the calculated vibrational modes, irrespective of their Raman activity. The comparison shows an overall agreement between theory and experiment, although the computed relative intensities show deviations for some of the Raman active modes. We attribute these deviations mainly to resonant effects, since the experimental spectrum has been measured at laser wavelengths close to the energy of the electronic transition (at 1.58 eV). An important feature of the Raman spectra of the heated samples is the presence of additional peaks at the frequency values of 458 and 1240 cm^{-1}. The experimental spectrum of the CoPc molecule shows no peaks on these positions. Moreover, the computational results show the absence of any vibrational modes (black stripes in Fig. 3) in the vicinity of these values, which points at the appearance of new vibration types upon heating of the samples. To investigate the possible source of these new vibrations we consider 3 hypothetical CoPc dimer structures with different degree of polymerization as approximates for prolonged CoPc polymers. The proposed model structures represent two CoPc molecules connected with one, two and four C-C bonds, and are labeled as type 1, type 2 and type 3, respectively (see Fig. 4).

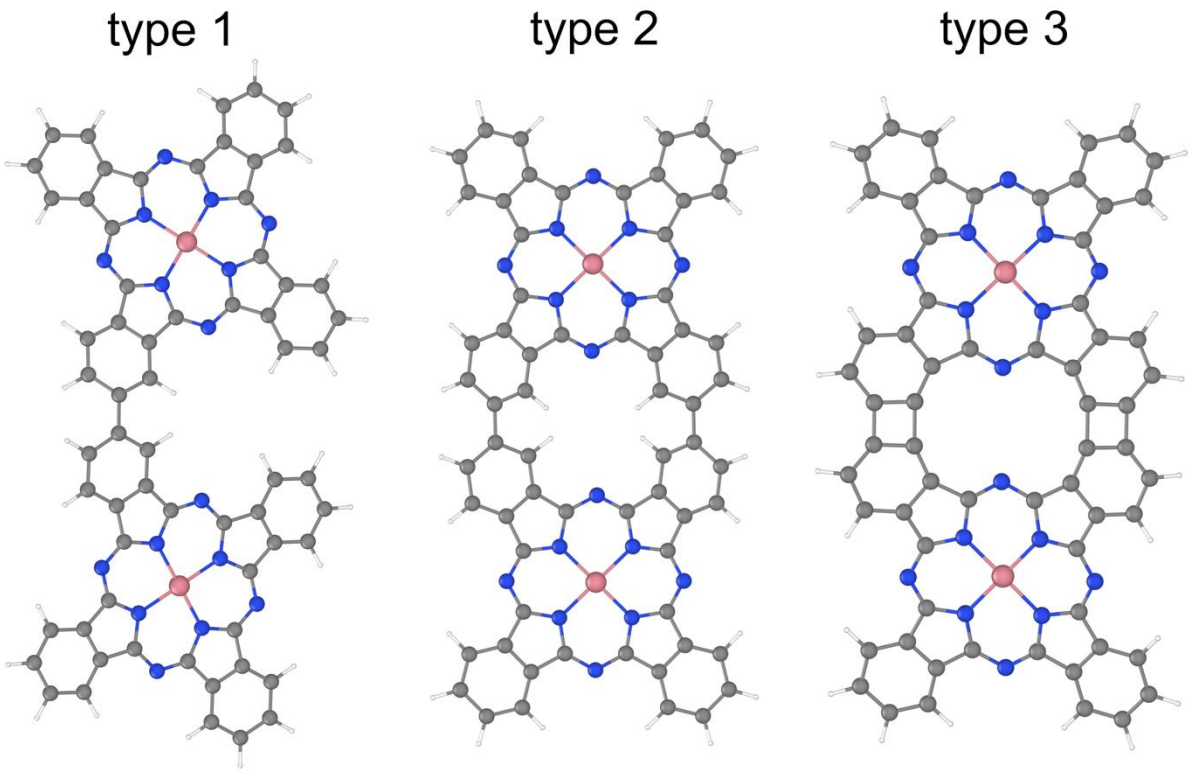

Figure 4. Models of molecules polymerization in dimer configuration. The atomic structure of hypothetical CoPc dimers with different degree of polymerization considered in the simulations.

After applying the same scaling factor for calculated vibrational frequencies we find the best agreement of calculated and experimental spectra for the type 2 structure (see Fig. 5a). The important feature of the theoretical spectrum of the type 2 structure is the presence of Raman peaks at frequencies of 453 and 1239 cm^{-1}, close to the corresponding new peaks in the annealed samples. The eigen displacements of these two vibrational modes are localized in the vicinity of the connection points of the two CoPc molecules (see Fig. 5b) and may be therefore considered as a signature of polymerization.

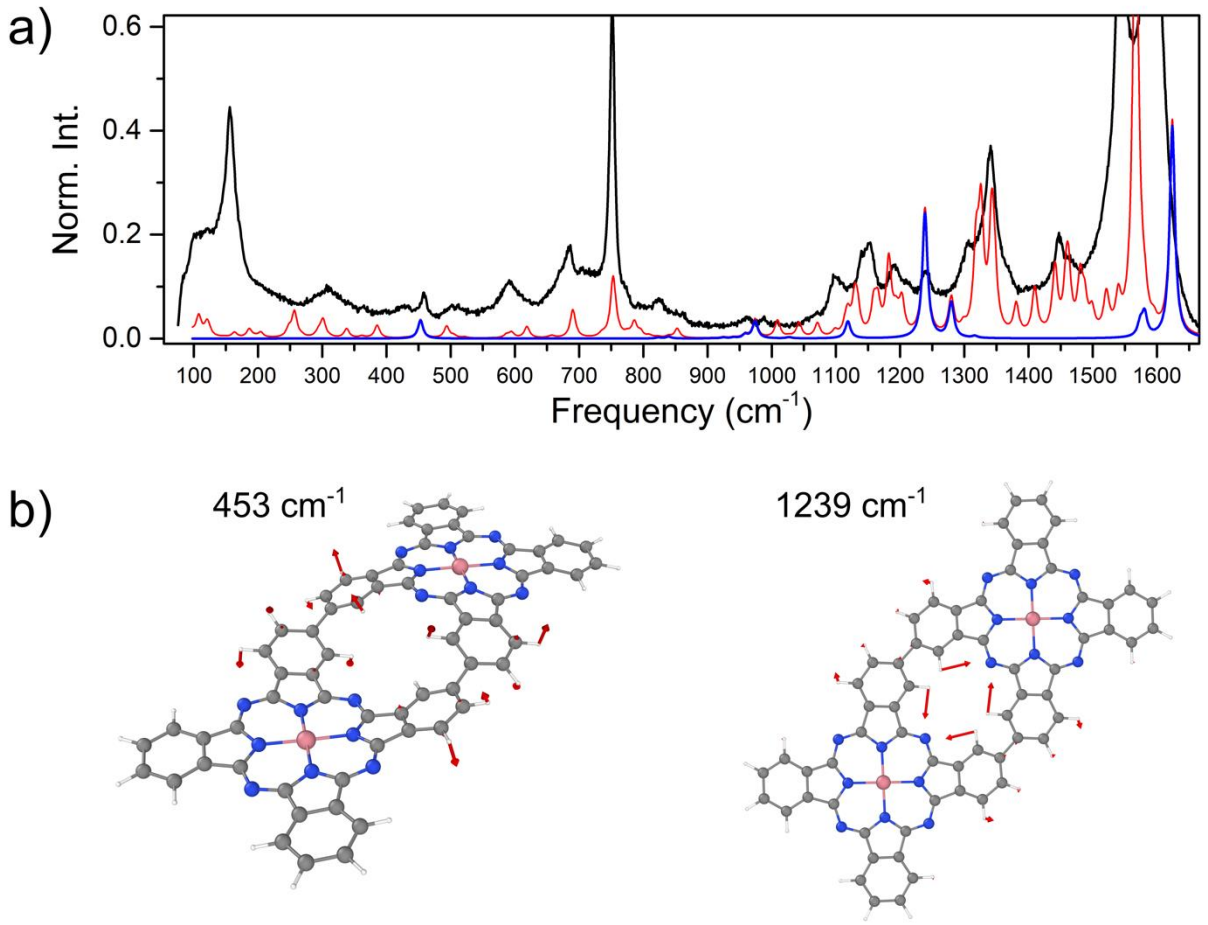

Figure 5. Comparison of Raman spectra and corresponding modes of vibrations. a) Comparison of experimental (black line) for 600 °C polymerization and calculated (red line) Raman spectra for the CoPc type 2 dimer. The blue line depicts the projected spectrum that takes into account only vibrations localized around the molecule connection points. b) Eigen displacements of the modes of interest.

In order to identify the overall impact of such local vibrations on the Raman spectrum, we perform a projection procedure in which we consider the contribution of only the vibrational modes that have at least 90 % of the atomic displacements near the molecule's connection points. The corresponding spectrum is shown in Fig. 5a (blue line). Besides the two above mentioned modes, we also find finite intensity bands at frequency values of 974, 1119, 1280, 1580 and 1624

cm^{-1}. These additional modes that originate from the atomic displacements localized around CoPc molecule's connection points, could not however be successfully resolved in the experiment due to their overlap with the other Raman modes. Our simulations suggest, therefore, that the changes of the Raman spectrum upon heating of the encapsulated CoPc molecules can be attributed to the polymerization of the molecules and the new Raman modes may be a specific feature of the vibrations around the molecule connection points.

Optical absorption properties of CoPcNRs

We now turn to the discussion of the optical absorption of the synthesized materials in the visible and near IR ranges. In Fig. 6a we represent the absorption spectra of pristine SWCNTs and nanotubes after the filling protocol and polymerization step at 500 °C. For pristine SWCNTs one can detect the E_{11} transition band for semiconducting tubes (1600-2350 nm), E_{22s} (1000-1350 nm), and E_{11} of metallic nanotubes (650-850 nm). Upon the filling of SWCNTs with CoPc molecules and polymerization of molecules into the NRs at 500 °C we detect the significant redshift of the E_{11s} band in comparison to pristine opened nanotubes. Large shifts of the central band position on 200 nm can be attributed to the modification of the nanotube cross section upon filling together with a dielectric screening by the encapsulated molecules and NRs[25]. A new band appears in the spectra of the filled samples in the visible range close to the E_{11m} region. Due to the high intensity the new band can be clearly observed around 700 nm. We also performed a comparison between the spectra for the filled nanotubes and not fully polymerized molecules (sample at 390 °C) and for the case of the optimal conditions for the formation of CoPcNRs at 500 °C (see supporting information). We note the red shift of the new band for CoPcNR sample and suppose that this spectral feature at 715 nm is the fingerprint of CoPcNRs in absorption spectrum.

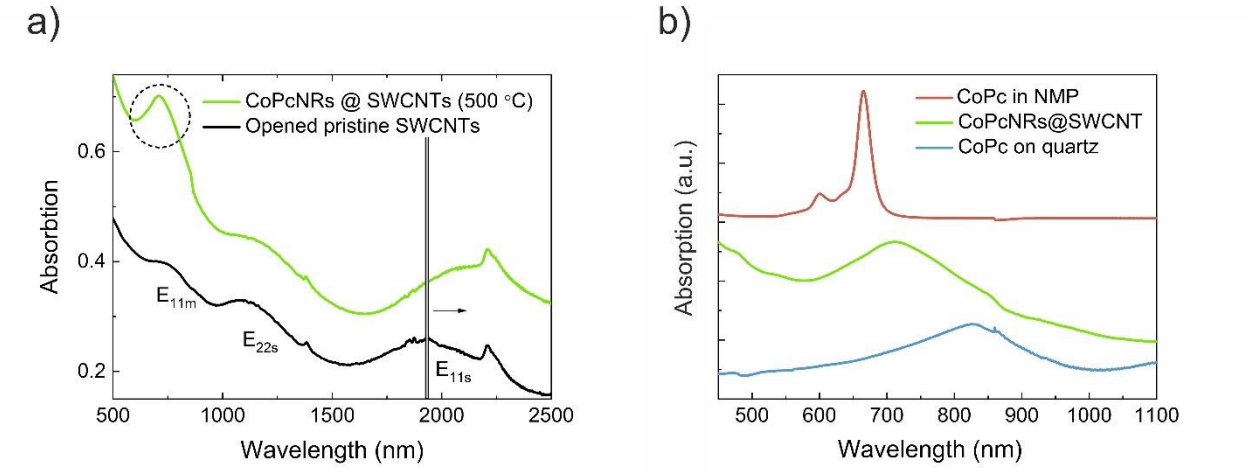

Figure 6. Optical absorption measurements. (a) Absorption measurements of opened pristine SWCNTs (black) and filled with CoPcNRs (green color). Dashed circle highlights the appearance of the new broad feature similar to the Q-band of CoPc. (b) Comparison of absorption spectra of CoPc molecules in NMP (red, liquid phase), CoPcNRs (green, solid phase; response of SWCNTs was subtracted for this spectrum), and similarly processed CoPc without nanotubes (blue color, solid phase).

When we take a closer look at the visible range and compare the optical spectra of pristine CoPc molecules, we observe molecules that underwent the same temperature modification but without the nanotube supporting matrix, and CoPcNRs that were grown inside the SWCNTs (Fig. 6b). Optical absorption spectrum of CoPc in N-Methyl-2-pyrrolidone (NMP) solution exhibits well defined bands with resonances at 665 and 600 nm. The resonance at 665 nm corresponds to $\pi \rightarrow \pi^*$ electronic transition (Q-band of CoPc) while the latter one is associated with vibration satellite of the Q-band. Phthalocyanine compounds tend to aggregate in thin films and even in diluted solutions[40,41]. The aggregation process is accompanied with pronounced change in optical properties. Aggregates typically demonstrate specific absorption bands in the UV-Vis spectra. Conventionally, there are H and J phthalocyanine aggregates[42] in organic materials. H aggregates

provide hypsochromic (blue) shift of the Q-band of monomers while bathochromic (red) shifts are present for J-aggregates. The spectral shift occurs due to intermolecular interactions between phthalocyanine molecules, as explained by the molecular exciton theory proposed by Kasha[43]. Commonly, both types of the aggregates exist in thin films formed by thermal evaporation techniques[44]. As a result, Q-band gets spectrally broadened and red-shifted. As it is depicted in Fig. 6b absorption Q-band of CoPc film on quartz is bathochromically shifted from 665 to 825 nm and broadened (FWHM from 40 nm in NMP up to 110 nm on the substrate). Optical properties of narrow sub-nanometer GNRs strongly depend on the width, geometry and atoms on the edges. In the case of semiconducting GNRs the bang gap is inversely proportional to the width of the ribbon. For instance, a well reproduced 7-AGNRs exhibit absorption bands at 620 nm (2 eV) and larger[26,39], which are assigned to the excitonic transitions. In Fig. 6b we plot the CoPcNR spectrum with the subtracted contribution from pristine SWCNT. The absorption band at 715 nm (1.7 eV) can be clearly observed. Since the absorption peak overlaps at long wavelengths with the E_{11m} band of the nanotubes, it is complicated to estimate correctly the FWHM value, but in general that is less than the values in the case of the stacked CoPc molecules deposited from the gas phase on the substrate. The absorption peak at 715 nm becomes the fingerprint of the formed CoPcNRs, which can be traced back to the original Q-band of the CoPc molecules that serve as the starting material for the synthesis of NRs. The absorption peak of CoPcNRs is spectrally shifted, with respect to both pristine suspended and stacked on the substrate molecules, since CoPcs get linked in the specific fashion inside the 1D nanotube core.

Magnetic properties of CoPcNR

Magnetic GNRs inside SWCNTs potentially have several advantages since they are aligned within the nanotube channels and protected by them. An additional advantage is that these hybrid materials can be processed with the well-established techniques implemented for nanotubes. Since the encapsulation inside SWCNTs allows for the optical excitation[45,46] and probing the state of the inner structures[47], the magnetic state can also be studied optically in the similar fashion to 2D magnetic layers[48]. Magnetic properties of the CoPcNR inside SWCNT were investigated by transverse magnetooptical Kerr effect measurements (TMOKE). TMOKE is an intensity magneto-optical effect linear in magnetization, which makes it possible to characterize the magnetic properties of materials. It is an efficient tool for the investigation magnetic properties of low dimensional materials[49]. The general formulae for TMOKE[50] takes the following form:

$$\delta = \frac{\Delta I}{I(0)} \qquad (1)$$

where $\Delta I = I(M) - I(-M)$, $I(M)$ is the intensity of the light reflected from the magnetized sample, $I(0)$ - intensity of light reflected from a non-magnetized sample.

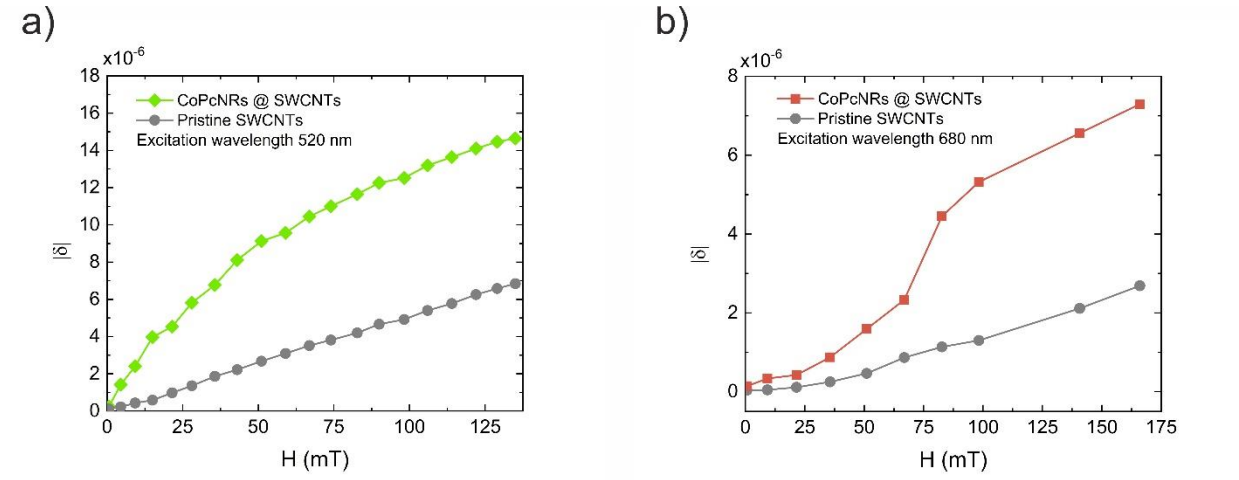

Figure 7. Magnetic properties of CoPcNRs probed by TMOKE. (a). TMOKE measurements from pristine nanotubes (gray color) and CoPcNRs polymerized inside SWCNTs (green color). Laser

excitation at 520 nm. (b). TMOKE signals for pristine nanotubes (gray color) and CoPcNRs polymerized inside SWCNTs (red color) obtained with the 680 nm wavelength laser excitation.

Magnetic properties of CoPc arise from unpaired spins in 3d orbitals of Co atoms. CoPc molecule possesses *ca.* 5 times smaller magnetic moment than Co^{2+} atoms[51,52]. As a free molecule CoPc has a spin ½ ground state and is paramagnetic, magnetic properties of CoPc films strongly depend on molecular organization[53] resulting from ferromagnetic to antiferromagnetic coupling[54]. For instance, α-CoPc has antifferomagnetic coupling in contrast to β-CoPc which possesses weak antiferromagnetic coupling[54]. For both configurations hysteresis loops at low temperatures (2 K) has paramagnetic behavior in a wide range of magnetic fields (from 0 to 7 T).

The magnetooptical response of pristine SWCNTs was linear and had the diamagnetic origin[19]. The dependences of TMOKE measured both at 520 and 680 nm for CoPcNRs at SWCNTs on the external magnetic field demonstrate hysteresis curves without saturation in the measured field ranges (Fig. 7). However, the TMOKE magnitude of the hybrid system is several times higher compared to pristine SWCNTs indicating contribution from Co atoms. Notably, the amplitude of the TMOKE signal at 520 nm is *ca.* 2 times higher than at 680 nm which can be caused by increased absorption at 680 nm (see Fig. 6a). The TMOKE curve behavior observed in our experiment at room temperature is paramagnetic for magnetic fields up to *ca.* 50 mT for measurements at both wavelengths. Above 50 mT, a magnetic response curve bend is observed which is believed to lead to saturation typically shown for ferromagnetic materials. The assumption is also supported by the ferromagnetic spin ordering obtained by numerical simulations for CoPc chains. However, in the case of α and β phase of CoPc[54] magnetic response behavior was observed to be paramagnetic for low temperatures and strong antiferromagnetic coupling for temperatures around 100 K. Notably, even in the case of α-phase iron phthalocyanine (FePc) both on sapphire and gold/sapphire

substrates magnetic hysteresis loops have paramagnetic behavior for temperatures higher than 25 K[55]. In the FePc case, the iron atoms couple ferromagnetically along quasi-one-dimensional chains (similar to the CoPcNR structure)[56]. In this respect, we believe, that stable magnetic ordering and magnetization saturation can be revealed for CoPcNR at lower temperatures and requires further investigation.

Conclusions

We demonstrate that CoPc molecules can fill 2 nm wide SWCNTs from the vapor phase and further be polymerized to form magnetic CoPcNRs inside. We determined the optimal synthesis parameters for successful polymerization process. By thorough analysis of Raman and UV-Vis-NIR spectroscopies studies, TEM imaging, and supported by DFT calculations we identified the fingerprint features of CoPcNRs and confirmed its encapsulation inside SWCNTs. For the DFT results on the phonon vibrational modes of several types of CoPc polymerization configurations, a projection procedure was implemented. It enables us to reveal that the Raman fingerprints that appear for CoPcNRs are attributed to the vibrations around the molecules connection points within a ribbon. The new phonon vibration modes that were clearly resolved in the experiments are located at frequencies of 453 and 1239 cm^{-1}. An impact of magnetic Co atoms was verified using TMOKE measurements at room temperature. The results displayed enhanced (up to 3 times) magnetic response with tendency to saturation commonly observed for ferromagnetic materials. We believe that being protected by the SWCNT and aligned along the 1D channel, CoPcNRs can be used for applications that require addressed control over the regularly distributed spins. The proposed principle of magnetic nanoribbon formation can be extrapolated for other phthalocyanine molecules which possess various magnetic properties with ferromagnetic or antiferromagnetic

coupling between magnetic atoms. The demonstrated material opens up opportunities for the development of a diverse class of protected low-dimensional magnetic materials for applications in organic spintronic, magnonic, and quantum devices.

Materials and methods

CoPcNR synthesis

SWCNTs with average diameter of around 2.1 nm grown by eDIPS method[57] and TuBall™ samples were used as templates for synthesis of the CoPcNRs. Purification was achieved by oxidation in air at 400 °C and then by acid treatment to remove the catalytic particles and amorphous carbon. Rinsing and filtering the SWCNT suspension by deionized water and ethanol for several times and finally SWCNT buckypaper was obtained after drying. To open the SWCNTs, the buckypaper was burned in air at 450 °C for 30 min. To fill the CoPc inside the opened SWCNTs, CoPc powder (Aladdin, 20 mg) was sealed together with the SWCNTs (around 2 mg) in a glass ampoule at pressure of 2.3×10^{-4} Pa, and then heated up at 375 °C for 3 days. Transforming the CoPc molecules into CoPcNRs inside the tubes was achieved by annealing at various temperatures for 1h in dynamic vacuum with base pressure better than 10^{-4} Pa. In the meantime, the CoPc molecules, which might be attached to the outside of the SWCNTs, can be removed through evaporation.

DFT calculations

The calculations for CoPc dimers were performed at the density functional theory level using the Becke three parameter hybrid functional with the non-local correlation functional of Lee-Yang-Parr (B3LYP)[58,59] together with 6-311G(d,p)[60] basis for non-metal atoms and LANL2DZ[61] for Co

atoms. as implemented in the Gaussian16 package[62]. Raman intensities were obtained within the same package using the numerical differentiation of dipole derivatives with respect to the electric field. To determine the favorable magnetic ordering, results of two calculations were compared for each type of polymerization: one for parallel spins on metal atoms and one for antiparallel ones[63].

TEM Measurements

SWCNTs filled with the encapsulated materials were dispersed in propan-2-ol using an ultrasonic bath and drop cast onto lacey carbon-coated copper TEM grids (Agar). HRTEM imaging was carried out on a JEOL 2100 FEG-TEM microscope operated at 200 kV.

EDX spectroscopy

Local EDX spectra were acquired for samples mounted on TEM grids using an Oxford Instruments INCA X-ray microanalysis system. The electron beam was condensed onto areas of specimens (bulk specimen or nanotube bundles) suspended over holes of the amorphous carbon film.

Raman spectroscopy

Raman spectra (Renishaw, inVia Reflex) was recorded at ambient conditions under an objective of x50 (NA=0.5) by using a laser with wavelength of 785 nm (E =1.58 eV) for excitation at a power of 1 mW to exclude any heating effect on the samples. Considering the focal length of the spectrometer and the grating of 1600 Grooves/mm, the spectral resolution was around 2 wavenumbers.

UV-Vis-NIR absorption measurements

Absorption measurements (Cary 5000 UV-Vis-NIR spectrometer) were performed on the samples in the solid form deposited on quartz substrates, otherwise mentioned explicitly. In the case when the samples initially were in the form of bucky papers the deposition on quartz substrates was performed via vacuum filtration on the mixed cellulose filters. For the liquid samples the quartz cuvettes with 10 x 5 mm dimensions have been used.

TMOKE measurements

All TMOKE measurements were carried out at the room temperature. The samples were in the solid-state form deposited on the quartz substrates. For the magnetic measurements initial nanotube films were deposited on quartz, then opened, filled, and polymerized. It allowed to obtain filled and pristine nanotubes with the exact same thickness in order to perform the quantitative measurements. The samples were irradiated with the light of laser diode with 520 and 680 nm wavelength. The radius of laser beam was 100 um. The plane of incidence of light was perpendicular to the direction of the external magnetic field and an external magnetic field was modulated by sinusoidal signal with a frequency of 92 Hz. The laser beam reflected from the sample passed through the Wollaston prism, where it was divided into two beams with p- and s-polarizations. The absolute value of intensity difference $|\Delta I|$ of p- and s-polarized beams was measured using a balanced photodetector.

AUTHOR INFORMATION

Corresponding Author

* Alexander I. Chernov email: chernov.ai@mipt.ru

Author Contributions

LS, YW, PF, and AC fabricated the CoPcNRs and studied the Raman spectra. DK, PF, and AC performed the optical spectroscopy studies. PF and EO participated in interpretation of optical absorption data of molecules. PK, PS, and VB contributed to the magnetic measurements. KF, CS, and AK performed the HRTEM studies and EDX measurements. VB and DR performed the calculations of the Raman spectra. AC planned the research and organized the experimental work. All co-authors contributed to the discussion of the data. DK, DR, and AC wrote the manuscript. All authors have given approval to the final version of the manuscript.

ACKNOWLEDGMENT AND FUNDING SOURCES

We thank Takeshi Saito for supplying the eDIPS SWCNTs. LS acknowledges the financial support from the National Natural Science Foundation of China (Grant 51902353) and Natural Science Foundation of Guangdong Province (Grant 2019A1515011227). DVR acknowledges support from Russian Ministry of Science and Higher Education (Grant No. 2711.2020.2 to leading scientific schools). PVF acknowledges the financial support from RFBR 19-32-60006, for funding part of the experiments on filling nanotubes. VIB acknowledges RFBR 18-29-20113. Computations of atomic structure and Raman spectra of CoPc dimers were supported by RSF 19-72-30043 project. The modeling of interaction between the CoPc molecule and carbon nanotube was done within the Project of the State Assignment (Vernadsky Institute of Geochemistry and Analytical Chemistry of Russian Academy of Sciences, Moscow, Russian Federation).

CONFLICT OF INTEREST

Authors declare no conflict of interests.

REFERENCES

(1) Leisegang, M.; Christ, A.; Haldar, S.; Heinze, S.; Bode, M. Molecular Chains: Arranging and Programming Logic Gates. *Nano Letters* **2021**, *21* (1), 550–555. https://doi.org/10.1021/acs.nanolett.0c03984.

(2) Zhang, X.; Wang, Y.; Gu, M.; Wang, M.; Zhang, Z.; Pan, W.; Jiang, Z.; Zheng, H.; Lucero, M.; Wang, H.; Sterbinsky, G. E.; Ma, Q.; Wang, Y. G.; Feng, Z.; Li, J.; Dai, H.; Liang, Y. Molecular Engineering of Dispersed Nickel Phthalocyanines on Carbon Nanotubes for Selective CO2 Reduction. *Nature Energy* **2020**, *5* (9), 684–692. https://doi.org/10.1038/s41560-020-0667-9.

(3) Li, T.; Bandari, V. K.; Hantusch, M.; Xin, J.; Kuhrt, R.; Ravishankar, R.; Xu, L.; Zhang, J.; Knupfer, M.; Zhu, F.; Yan, D.; Schmidt, O. G. Integrated Molecular Diode as 10 MHz Half-Wave Rectifier Based on an Organic Nanostructure Heterojunction. *Nature Communications* **2020**, *11* (1), 1–10. https://doi.org/10.1038/s41467-020-17352-9.

(4) Coronado, E. Molecular Magnetism: From Chemical Design to Spin Control in Molecules, Materials and Devices. *Nature Reviews Materials* **2020**, *5* (2), 87–104. https://doi.org/10.1038/s41578-019-0146-8.

(5) Kroll, T.; Aristov, V. Y.; Molodtsova, V.; Ossipyan, Y. A.; Vyalikh, D. V.; Büchner, B.; Knupfer, M. Spin and Orbital Ground State of Co in Cobalt Phthalocyanine. *Journal of Physical Chemistry A* **2009**, *113* (31), 8917–8922. https://doi.org/10.1021/jp903001v.

(6) Barraud, C.; Bouzehouane, K.; Deranlot, C.; Kim, D. J.; Rakshit, R.; Shi, S.; Arabski, J.; Bowen, M.; Beaurepaire, E.; Boukari, S.; Petroff, F.; Seneor, P.; Mattana, R. Phthalocyanine Based Molecular Spintronic Devices. *Dalton Transactions* **2016**, *45* (42), 16694–16699. https://doi.org/10.1039/c6dt02467j.

(7) Cinchetti, M.; Dediu, V. A.; Hueso, L. E. Activating the Molecular Spinterface. *Nature Materials* **2017**, *16* (5), 507–515. https://doi.org/10.1038/nmat4902.

(8) Thiele, S., Balestro, F., Ballou, R., Klyatskaya, S., Ruben, M., Wernsdorfer, W. Electrically Driven Nuclear Spin Resonance in Single-Molecule Magnets. **2014**, *344* (6188). https://doi.org/10.1126/science.1249802.

(9) Atzori, M.; Tesi, L.; Morra, E.; Chiesa, M.; Sorace, L.; Sessoli, R. Room-Temperature Quantum Coherence and Rabi Oscillations in Vanadyl Phthalocyanine: Toward Multifunctional Molecular Spin Qubits. *Journal of the American Chemical Society* **2016**, *138* (7), 2154–2157. https://doi.org/10.1021/jacs.5b13408.

(10) Warner, M.; Din, S.; Tupitsyn, I. S.; Morley, G. W.; Stoneham, A. M.; Gardener, J. A.; Wu, Z.; Fisher, A. J.; Heutz, S.; Kay, C. W. M.; Aeppli, G. Potential for Spin-Based Information Processing in a Thin-Film Molecular Semiconductor. *Nature* **2013**, *503* (7477), 504–508. https://doi.org/10.1038/nature12597.

(11) Aromí, G.; Aguilà, D.; Gamez, P.; Luis, F.; Roubeau, O. Design of Magnetic Coordination Complexes for Quantum Computing. *Chemical Society Reviews* **2012**, *41* (2), 537–546. https://doi.org/10.1039/c1cs15115k.

(12) Lunghi, A.; Totti, F.; Sessoli, R.; Sanvito, S. The Role of Anharmonic Phonons in Under-Barrier Spin Relaxation of Single Molecule Magnets. *Nature Communications* **2017**, *8*. https://doi.org/10.1038/ncomms14620.

(13) Liu, F.; Krylov, D. S.; Spree, L.; Avdoshenko, S. M.; Samoylova, N. A.; Rosenkranz, M.; Kostanyan, A.; Greber, T.; Wolter, A. U. B.; Büchner, B.; Popov, A. A. Single Molecule Magnet with an Unpaired Electron Trapped between Two Lanthanide Ions inside a Fullerene. *Nature Communications* **2017**, *8* (May). https://doi.org/10.1038/ncomms16098.

(14) Nakanishi, R.; Satoh, J.; Katoh, K.; Zhang, H.; Breedlove, B. K.; Nishijima, M.; Nakanishi, Y.; Omachi, H.; Shinohara, H.; Yamashita, M. DySc2N@C80 Single-Molecule Magnetic Metallofullerene Encapsulated in a Single-Walled Carbon Nanotube. *Journal of the American Chemical Society* **2018**, *140* (35), 10955–10959. https://doi.org/10.1021/jacs.8b06983.

(15) Domanov, O.; Weschke, E.; Saito, T.; Peterlik, H.; Pichler, T.; Eisterer, M.; Shiozawa, H. Exchange Coupling in a Frustrated Trimetric Molecular Magnet Reversed by a 1D Nano-Confinement. *Nanoscale* **2019**, *11* (22), 10615–10621. https://doi.org/10.1039/C9NR00796B.

(16) Villalva, J.; Develioglu, A.; Montenegro-Pohlhammer, N.; Sánchez-de-Armas, R.; Gamonal, A.; Rial, E.; García-Hernández, M.; Ruiz-Gonzalez, L.; Costa, J. S.; Calzado, C. J.; Pérez, E. M.; Burzurí, E. Spin-State-Dependent Electrical Conductivity in Single-Walled Carbon Nanotubes Encapsulating Spin-Crossover Molecules. *Nature Communications* **2021**, *12* (1), 1–8. https://doi.org/10.1038/s41467-021-21791-3.

(17) Khlobystov, A. N. Carbon Nanotubes: From Nano Test Tube to Nano-Reactor. *ACS Nano* **2011**, *5* (12), 9306–9312. https://doi.org/10.1021/nn204596p.

(18) Cleuziou, J.-P.; Wernsdorfer, W.; Ondarçuhu, T.; Monthioux, M. Electrical Detection of Individual Magnetic Nanoparticles Encapsulated in Carbon Nanotubes. *ACS Nano* **2011**, *5* (3), 2348–2355. https://doi.org/10.1021/nn2000349.

(19) Briones-Leon, A.; Ayala, P.; Liu, X.; Yanagi, K.; Weschke, E.; Eisterer, M.; Jiang, H.; Kataura, H.; Pichler, T.; Shiozawa, H. Orbital and Spin Magnetic Moments of Transforming

One-Dimensional Iron inside Metallic and Semiconducting Carbon Nanotubes. *Physical Review B* **2013**, *87* (19), 195435. https://doi.org/10.1103/PhysRevB.87.195435.

(20) Okotrub, A. V; Chernov, A. I.; Lavrov, A. N.; Gurova, O. A.; Shubin, Y. V; Palyanov, Y. N.; Borzdov, Y. M.; Zvezdin, A. K.; Lähderanta, E.; Bulusheva, L. G.; Sedelnikova, O. V. Magnetic Properties of 1D Iron–Sulfur Compounds Formed Inside Single-Walled Carbon Nanotubes. *physica status solidi (RRL) – Rapid Research Letters* **2020**, *14* (10), 2000291. https://doi.org/https://doi.org/10.1002/pssr.202000291.

(21) Li, L. J.; Khlobystov, A. N.; Wiltshire, J. G.; Briggs, G. A. D.; Nicholas, R. J. Diameter-Selective Encapsulation of Metallocenes in Single-Walled Carbon Nanotubes. *Nature Materials* **2005**, *4* (6), 481–485. https://doi.org/10.1038/nmat1396.

(22) Anoshkin, I. V; Talyzin, A. V; Nasibulin, A. G.; Krasheninnikov, A. V; Jiang, H.; Nieminen, R. M.; Kauppinen, E. I. Coronene Encapsulation in Single-Walled Carbon Nanotubes: Stacked Columns, Peapods, and Nanoribbons. *ChemPhysChem* **2014**, *15* (8), 1660–1665. https://doi.org/10.1002/cphc.201301200.

(23) Chernov, A. I.; Fedotov, P. V.; Anoshkin, I. V.; Nasibulin, A. G.; Kauppinen, E. I.; Kuznetsov, V. L.; Obraztsova, E. D. Single-Walled Carbon Nanotubes as a Template for Coronene Stack Formation. *Physica Status Solidi (B) Basic Research* **2014**, *251* (12), 2372–2377. https://doi.org/10.1002/pssb.201451159.

(24) Talyzin, A. V; Anoshkin, I. V; Krasheninnikov, A. V; Nieminen, R. M.; Nasibulin, A. G.; Jiang, H.; Kauppinen, E. I. Synthesis of Graphene Nanoribbons Encapsulated in Single-Walled Carbon Nanotubes. *Nano Letters* **2011**, *11* (10), 4352–4356. https://doi.org/10.1021/nl2024678.

(25) Chernov, A. I.; Fedotov, P. V; Lim, H. E.; Miyata, Y.; Liu, Z.; Sato, K.; Suenaga, K.; Shinohara, H.; Obraztsova, E. D. Band Gap Modification and Photoluminescence Enhancement of Graphene Nanoribbon Filled Single-Walled Carbon Nanotubes. *Nanoscale* **2018**, *10* (6), 2936–2943. https://doi.org/10.1039/C7NR07054C.

(26) Denk, R.; Hohage, M.; Zeppenfeld, P.; Cai, J.; Pignedoli, C. A.; Söde, H.; Fasel, R.; Feng, X.; Müllen, K.; Wang, S.; Prezzi, D.; Ferretti, A.; Ruini, A.; Molinari, E.; Ruffieux, P. Exciton-Dominated Optical Response of Ultra-Narrow Graphene Nanoribbons. *Nature Communications* **2014**, *5*, 4253. https://doi.org/10.1038/ncomms5253.

(27) Falke, Y.; Senkovskiy, B. V; Ehlen, N.; Wysocki, L.; Marangoni, T.; Durr, R. A.; Chernov, A. I.; Fischer, F. R.; Grüneis, A. Photothermal Bottom-up Graphene Nanoribbon Growth Kinetics. *Nano Letters* **2020**, *20* (7), 4761–4767. https://doi.org/10.1021/acs.nanolett.0c00317.

(28) Chuvilin, A.; Bichoutskaia, E.; Gimenez-Lopez, M. C.; Chamberlain, T. W.; Rance, G. A.; Kuganathan, N.; Biskupek, J.; Kaiser, U.; Khlobystov, A. N. Self-Assembly of a Sulphur-Terminated Graphene Nanoribbon within a Single-Walled Carbon Nanotube. *Nature Materials* **2011**, *10* (9), 687–692. https://doi.org/10.1038/nmat3082.

(29) Kuzmany, H.; Shi, L.; Martinati, M.; Cambré, S.; Wenseleers, W.; Kürti, J.; Koltai, J.; Kukucska, G.; Cao, K.; Kaiser, U.; Saito, T.; Pichler, T. Well-Defined Sub-Nanometer Graphene Ribbons Synthesized inside Carbon Nanotubes. *Carbon* **2021**, *171*, 221–229. https://doi.org/10.1016/j.carbon.2020.08.065.

(30) Sun, Q.; Yao, X.; Gröning, O.; Eimre, K.; Pignedoli, C. A.; Müllen, K.; Narita, A.; Fasel, R.; Ruffieux, P. Coupled Spin States in Armchair Graphene Nanoribbons with Asymmetric Zigzag Edge Extensions. *Nano Letters* **2020**, *20* (9), 6429–6436. https://doi.org/10.1021/acs.nanolett.0c02077.

(31) Tong, W. Y.; Djurišić, A. B.; Xie, M. H.; Ng, A. C. M.; Cheung, K. Y.; Chan, W. K.; Leung, Y. H.; Lin, H. W.; Gwo, S. Metal Phthalocyanine Nanoribbons and Nanowires. *The Journal of Physical Chemistry B* **2006**, *110* (35), 17406–17413. https://doi.org/10.1021/jp062951q.

(32) Chamberlain, T. W.; Biskupek, J.; Rance, G. A.; Chuvilin, A.; Alexander, T. J.; Bichoutskaia, E.; Kaiser, U.; Khlobystov, A. N. Size, Structure, and Helical Twist of Graphene Nanoribbons Controlled by Confinement in Carbon Nanotubes. *ACS Nano* **2012**, *6* (5), 3943–3953. https://doi.org/10.1021/nn300137j.

(33) Chamberlain, T. W.; Biskupek, J.; Skowron, S. T.; Markevich, A. v; Kurasch, S.; Reimer, O.; Walker, K. E.; Rance, G. A.; Feng, X.; Müllen, K.; Turchanin, A.; Lebedeva, M. A.; Majouga, A. G.; Nenajdenko, V. G.; Kaiser, U.; Besley, E.; Khlobystov, A. N. Stop-Frame Filming and Discovery of Reactions at the Single-Molecule Level by Transmission Electron Microscopy. *ACS Nano* **2017**, *11* (3), 2509–2520. https://doi.org/10.1021/acsnano.6b08228.

(34) Pollack, A.; Alnemrat, S.; Chamberlain, T. W.; Khlobystov, A. N.; Hooper, J. P.; Osswald, S. Electronic Property Modification of Single-Walled Carbon Nanotubes by Encapsulation of Sulfur-Terminated Graphene Nanoribbons. *Small* **2014**, *10* (24), 5077–5086. https://doi.org/https://doi.org/10.1002/smll.201401034.

(35) Jiang, Y.; Li, H.; Li, Y.; Yu, H.; Liew, K. M.; He, Y.; Liu, X. Helical Encapsulation of Graphene Nanoribbon into Carbon Nanotube. *ACS Nano* **2011**, *5* (3), 2126–2133. https://doi.org/10.1021/nn103317u.

(36) Ferrari, A. C.; Basko, D. M. Raman Spectroscopy as a Versatile Tool for Studying the Properties of Graphene. *Nature Nanotechnology* **2013**, *8* (4), 235–246. https://doi.org/10.1038/nnano.2013.46.

(37) Gillen, R.; Mohr, M.; Thomsen, C.; Maultzsch, J. Vibrational Properties of Graphene Nanoribbons by First-Principles Calculations. *Physical Review B - Condensed Matter and Materials Physics* **2009**, *80* (15), 1–9. https://doi.org/10.1103/PhysRevB.80.155418.

(38) Plank, W.; Pfeiffer, R.; Scharman, C.; Wirtz, L.; Calvaresi, M.; Zerbetto, F.; Meyer, J.; Kuzmany, H. Electronic Structure and Radial Breathing Mode for Carbon Nanotubes with Ultra-High Curvature. *Physica Status Solidi (B) Basic Research* **2010**, *247* (11–12), 2774–2778. https://doi.org/10.1021/nn100615d.

(39) Fedotov, P. V; Rybkovskiy, D. V; Chernov, A. I.; Obraztsova, E. A.; Obraztsova, E. D. Excitonic Photoluminescence of Ultra-Narrow 7-Armchair Graphene Nanoribbons Grown by a New "Bottom-Up" Approach on a Ni Substrate under Low Vacuum. *The Journal of Physical Chemistry C* **2020**, *124* (47), 25984–25991. https://doi.org/10.1021/acs.jpcc.0c07369.

(40) Chowdhury, A.; Biswas, B.; Majumder, M.; Sanyal, M. K.; Mallik, B. Studies on Phase Transformation and Molecular Orientation in Nanostructured Zinc Phthalocyanine Thin Films Annealed at Different Temperatures. *Thin Solid Films* **2012**, *520* (21), 6695–6704. https://doi.org/10.1016/j.tsf.2012.07.013.

(41) Krichevsky, D. M.; Zasedatelev, A. V.; Tolbin, A. Yu.; Luchkin, S. Yu.; Karpo, A. B.; Krasovskii, V. I.; Tomilova, L. G. Highly Transparent Low-Symmetry Zinc Phthalocyanine-Based Monolayers for NO 2 Gas Detection. *Thin Solid Films* **2017**, *642*, 295–302. https://doi.org/10.1016/j.tsf.2017.10.001.

(42) Eisfeld, A.; Briggs, J. S. The J- and H-Bands of Organic Dye Aggregates. *Chemical Physics* **2006**, *324* (2–3), 376–384. https://doi.org/10.1016/j.chemphys.2005.11.015.

(43) Kasha, M. Energy Transfer Mechanisms and the Molecular Exciton Model for Molecular Aggregates. *Radiation Research* **2012**, *178* (2), 55–70. https://doi.org/10.1667/RRAV03.1.

(44) El-Nahass, M. M.; El-Gohary, Z.; Soliman, H. S. Structural and Optical Studies of Thermally Evaporated CoPc Thin Films. *Optics and Laser Technology* **2003**, *35* (7), 523–531. https://doi.org/10.1016/S0030-3992(03)00068-9.

(45) Chernov, A. I.; Fedotov, P. V; Talyzin, A. V; Lopez, I. S.; Anoshkin, I. V; Nasibulin, A. G.; Kauppinen, E. I.; Obraztsova, E. D. Optical Properties of Graphene Nanoribbons Encapsulated in Single-Walled Carbon Nanotubes. *ACS Nano* **2013**, No. 7, 6346–6353.

(46) Van Bezouw, S.; Arias, D. H.; Ihly, R.; Cambré, S.; Ferguson, A. J.; Campo, J.; Johnson, J. C.; Defillet, J.; Wenseleers, W.; Blackburn, J. L. Diameter-Dependent Optical Absorption and Excitation Energy Transfer from Encapsulated Dye Molecules toward Single-Walled Carbon Nanotubes. *ACS Nano* **2018**, *12* (7), 6881–6894. https://doi.org/10.1021/acsnano.8b02213.

(47) Ma, X.; Cambré, S.; Wenseleers, W.; Doorn, S. K.; Htoon, H. Quasiphase Transition in a Single File of Water Molecules Encapsulated in (6,5) Carbon Nanotubes Observed by Temperature-Dependent Photoluminescence Spectroscopy. *Physical Review Letters* **2017**, *118* (2), 27402.

(48) Jiang, S.; Li, L.; Wang, Z.; Mak, K. F.; Shan, J. Controlling Magnetism in 2D CrI3 by Electrostatic Doping. *Nature Nanotechnology* **2018**, *13* (7), 549–553. https://doi.org/10.1038/s41565-018-0135-x.

(49) Yang, K.; Hu, W.; Wu, H.; Whangbo, M. H.; Radaelli, P. G.; Stroppa, A. Magneto-Optical Kerr Switching Properties of (CrI3)2and (CrBr3/CrI3) Bilayers. *ACS Applied Electronic Materials* **2020**, *2* (5), 1373–1380. https://doi.org/10.1021/acsaelm.0c00154.

(50) Zvezdin, A. K.; Kotov, V. A. *Modern Magnetooptics and Magnetooptical Materials*; CRC Press, 1997.

(51) Annese, E.; Fujii, J.; Vobornik, I.; Panaccione, G.; Rossi, G. Control of the Magnetism of Cobalt Phthalocyanine by a Ferromagnetic Substrate. *Physical Review B - Condensed Matter and Materials Physics* **2011**, *84* (17), 1–7. https://doi.org/10.1103/PhysRevB.84.174443.

(52) Chen, X.; Alouani, M. Effect of Metallic Surfaces on the Electronic Structure, Magnetism, and Transport Properties of Co-Phthalocyanine Molecules. *Physical Review B - Condensed Matter and Materials Physics* **2010**, *82* (9), 1–11. https://doi.org/10.1103/PhysRevB.82.094443.

(53) Wu, W.; Harrison, N. M.; Fisher, A. J. Electronic Structure and Exchange Interactions in Cobalt-Phthalocyanine Chains. *Physical Review B - Condensed Matter and Materials Physics* **2013**, *88* (2), 1–9. https://doi.org/10.1103/PhysRevB.88.024426.

(54) Serri, M.; Wu, W.; Fleet, L. R.; Harrison, N. M.; Hirjibehedin, C. F.; Kay, C. W. M.; Fisher, A. J.; Aeppli, G.; Heutz, S. High-Temperature Antiferromagnetism in Molecular Semiconductor Thin Films and Nanostructures. *Nature Communications* **2014**, *5*, 1–9. https://doi.org/10.1038/ncomms4079.

(55) Gredig, T.; Colesniuc, C. N.; Crooker, S. A.; Schuller, I. K. Substrate-Controlled Ferromagnetism in Iron Phthalocyanine Films Due to One-Dimensional Iron Chains. *Physical Review B - Condensed Matter and Materials Physics* **2012**, *86* (1), 1–6. https://doi.org/10.1103/PhysRevB.86.014409.

(56) Evangelisti, M.; Bartolomé, J.; de Jongh, L. J.; Filoti, G. Magnetic Properties of (Formula Presented)-Iron(II) Phthalocyanine. *Physical Review B - Condensed Matter and Materials Physics* **2002**, *66* (14), 1–11. https://doi.org/10.1103/PhysRevB.66.144410.

(57) Saito, T.; Ohshima, S.; Okazaki, T.; Ohmori, S.; Yumura, M.; Iijima, S. Selective Diameter Control of Single-Walled Carbon Nanotubes in the Gas-Phase Synthesis. *Journal of nanoscience and nanotechnology* **2008**, *8* (11), 6153–6157.

(58) Becke, A. D. Density-Functional Thermochemistry. III. The Role of Exact Exchange. *The Journal of Chemical Physics* **1993**, *98* (7), 5648–5652. https://doi.org/10.1063/1.464913.

(59) Lee, C.; Yang, W.; Parr, R. G. Development of the Colle-Salvetti Correlation-Energy Formula into a Functional of the Electron Density. *Physical review B* **1988**, *37* (2), 785.

(60) Krishnan, R.; Binkley, J. S.; Seeger, R.; Pople, J. A. Self-Consistent Molecular Orbital Methods. XX. A Basis Set for Correlated Wave Functions. *The Journal of Chemical Physics* **1980**, *72* (1), 650–654. https://doi.org/10.1063/1.438955.

(61) Hay, P. J.; Wadt, W. R. Ab Initio Effective Core Potentials for Molecular Calculations. Potentials for K to Au Including the Outermost Core Orbitale. *The Journal of Chemical Physics* **1985**, *82* (1), 299–310. https://doi.org/10.1063/1.448975.

(62) Frisch, M. J. GAUSSIAN16. Revision A. 03. Gaussian Inc., Wallingford, CT, USA. 2016.

(63) Noodleman, L.; Case, D. A.; Aizman, A. Broken Symmetry Analysis of Spin Coupling in Iron-Sulfur Clusters. *Journal of the American Chemical Society* **1988**, *110* (4), 1001–1005. https://doi.org/10.1021/ja00212a003.